Article

JOURNAL OF COMPOSITE MATERIALS

Journal of Composite Materials
2018, Vol. 52(6) 773–792

DOI: 10.1177/0021998317714317
journals.sagepub.com/home/jcm
SAGE

Optimal cure cycle parameters for minimizing residual stresses in fiber-reinforced polymer composite laminates

PH Shah[1], VA Halls[2], JQ Zheng[2] and RC Batra[1]

Abstract

The curing of a fiber-reinforced composite laminate in an autoclave generally induces residual stresses that may make the cured laminate curved. Here, we find optimal cure cycle parameters for asymmetric cross-ply laminates that (i) provide uniform and nearly complete curing of the laminate (i.e., the degree of curve is the same everywhere and equals at least 0.96) within a specified time period and (ii) minimize residual stresses without adversely affecting the transverse effective elastic modulus of the laminate. We simulate the cure process by using functionalities built in the commercial finite element software ABAQUS, the cure process modeling software COMPRO and the multi-purpose software MATLAB. After having satisfactorily compared the presently computed results for the curing of two laminates with either experimental or numerical findings available in the literature, we use a genetic algorithm and the Latin hypercube sampling method to optimize the cure cycle parameters. It is found that in comparison to the manufacturer's recommended cure cycle (MRCC), for a cross-ply laminate with the span/thickness equal to 12.5, one optimal cycle reduces residual stresses by 47% and the total cure time from the MRCC time of 5 h to 4 h and another optimal cycle reduces the total cure time to 2 h and residual stresses by 8%. For the same cross-ply laminate with the span to thickness ratio of 125, an optimal cycle reduces the process induced curvature by 13% in comparison to the MRCC but increases the total cure time from 5 to 7.4 h. The approach presented here can be used by manufacturing engineers to obtain cure cycle parameters for fabricating composite laminates of desired quality.

Keywords

Cure process modeling, cure cycle optimization, genetic algorithm, residual stresses, composite laminate

Introduction

A common technique for fabricating fiber-reinforced polymer composite laminates is curing of resin pre-impregnated fibers (hereafter written as pre-pregs) in an autoclave under prescribed temperature and pressure cycles with the cycle parameters determining the quality of the cured laminate. Purslow and Childs[1] experimentally deduced optimal parameters of the cure cycle by fabricating several test panels until laminates with desired properties were produced. Holl and Rehfield[2] proposed real-time monitoring of cure cycle parameters using a control algorithm based on test results and physics of the process. The information about the physical state of the resin is collected during the cure process through sensors embedded in the laminate, and the cure cycle parameters (temperature and pressure) are adjusted in real time. However, as pointed out by Hubert and Poursartip,[3] this approach is expensive, and sensors are not only difficult to embed in a laminate but they also perturb the cure process and cannot be easily removed from the cured laminate. An effective and relatively inexpensive approach for determining cure cycle parameters is process modeling.

[1]Department of Biomedical Engineering and Mechanics, Virginia Polytechnic Institute and State University, USA
[2]US Army, Program Executive Office-Soldier, USA

Corresponding author:
RC Batra, Virginia Tech, 333E Norris Hall, Blacksburg, VA 24061, USA.
Email: rbatra@vt.edu

A mathematical model of the cure process that incorporates most, if not all, of the relevant physics yields a system of partial differential equations as well as initial and boundary conditions or equivalently an initial-boundary-value problem (IBVP) that is numerically solved for variables of interest. The validity of the mathematical model is established by comparing computed results with test observations. The input to the model includes[4] time histories of the autoclave temperature and pressure, material models for the resin and the fibers and the laminate geometry. The model output includes time histories of the degree of curve (DoC) of the resin, residual stresses in the cured laminate, the laminate shrinkage and thickness, the fiber (or resin) volume fraction and elastic moduli of the cured laminate. Effects of cure cycle parameters on the desired properties of the cured laminate are analyzed, and values of optimal cycle parameters are deduced that are verified through experiments.

One of the early process models developed by Loos and Springer[5] consists of three integrated sub-models, namely, the heat transfer considering internal heat generation, the resin flow including the laminate consolidation and residual stresses in the laminate. Loos and Springer[5] studied curing of unidirectional fiber-reinforced flat laminates made of thermosetting resin matrix and considered one-dimensional (1D) heat transfer in the thickness direction and the resin flow parallel to the fibers and along the laminate thickness. The temperature distributions and the resin flow determined by numerically solving the governing equations were found to agree with the corresponding experimental data.

Bogetti and Gillespie[6,7] developed cure models for thick (up to 7.62 cm thickness) thermosetting composites, proposed a constitutive relation for characterizing the material behavior that incorporates chemical hardening, dependence of the resin viscosity and moduli on the temperature and the DoC, thermal and cure shrinkage strains, and assumed fibers to be transversely isotropic about the longitudinal axis and the matrix to be isotropic. Initially, the uncured resin is assumed to behave as a viscous fluid. Subsequently, the resin stiffness increases and it undergoes chemical shrinkage, and finally when almost fully cured, it behaves as an elastic solid. The elastic parameters of fibers are assumed to remain constant throughout the cure process. The elastic moduli of the transversely isotropic cured composite were deduced by using a micromechanics approach from those of the fibers and the matrix and their volume fractions. By assuming that the material response is linear elastic during each time step and the matrix has different elastic moduli depending upon its DoC, they computed incremental strains and stresses during each time step and time histories of the laminate moduli.

Guo et al.[8] experimentally and numerically (using the finite element method (FEM)) studied curing of thick thermosetting matrix composite laminates and suggested that the manufacturer's recommended cure cycle (MRCC) be modified to reduce through-the-thickness temperature gradients in thick laminates and thereby improve upon the quality of the cured laminate. Ciriscioli et al.[9] experimentally measured the temperature, the ionic conductivity and the compaction (i.e., change in the laminate thickness) in graphite/epoxy laminates and showed that the MRCC gives temperature overshoot (i.e., temperature at an interior point in the laminate becomes significantly more than the surface temperature) and incomplete curing. They concluded that the MRCC should not be used to fabricate laminates of more than 52 plies for the ply thickness they used. The temperature overshoot introduces locally high temperature gradients which may adversely affect the laminate quality. Experimental results of Ciriscioli et al.[9] for the temperature and the thickness change agreed quantitatively with the corresponding numerical predictions from Loos and Springer's model[5] and that for the ionic conductivity agreed qualitatively with numerical solutions[5] of the resin DoC and the viscosity equations. Since the ionic conductivity is related to the DoC and the resin viscosity and no experimental technique for measuring the latter two parameters were available, they compared only trends for the three parameters. Hojjati and Hoa[10] developed a 1D cure model considering heat transfer and resin flow in the thickness direction and found that either the temperature overshot in the laminate or the incomplete compaction occurred using the MRCCs for thick laminates. They suggested that the consolidation can be improved by either bleeding the resin from both the top and the bottom surfaces of the laminate or by using a pre-bleeding technique in which first thin modules are compacted and then thick parts are fabricated by putting together the thin modules. Recently, Esposito et al.[11] experimentally found that the temperature overshoot in thick laminates reduces the interlaminar shear strength and proposed a model relating this reduction to the temperature of the exothermic peak. Sorrentino et al.[12] experimentally and numerically quantified the reduction in the interlaminar shear strength due to the temperature overshoot. They found that a temperature difference of 75°C between the two bounding surfaces of the laminate reduces the interlaminar shear strength by 17%.

White and Kim[13] developed a two-stage curing technique to address problems of thermal spiking and non-uniform consolidation in thick laminates. In stage 1, a thin stack of material is partially cured. Subsequently, another thin stack is placed on top of the first stack and the assembly is subjected to the stage 1 cure cycle.

This procedure is repeated until the laminate of the desired thickness is obtained and the final curing occurs in stage 2. They demonstrated that the staged curing reduces the void content and does not adversely affect the interlaminar shear strength and the mode-I fracture toughness. Kim and Lee[14] proposed a cure cycle with cooling and reheating steps and demonstrated that it reduces the temperature overshoot in thick laminates. The slopes of these two sequential steps were calculated by a trial and error approach. Oh and Lee[15] studied curing of glass/epoxy laminates using a 3D cure model and the FEM and found optimal values of the cure cycle parameters with cooling–reheating steps that minimize the temperature overshoot in the laminate. However, they did not consider constraints on the final DoC and its uniformity.

White and Hahn[16,17] developed a model to predict the cure induced residual stresses in the laminate by assuming the material to be linearly viscoelastic and accounting for chemical and thermal strains. By employing a least squares fit through experimental data for the graphite/bismaleimide (BMI) composite laminate, they deduced the major Poisson's ratio as an affine function of the DoC and the effective transverse modulus as a quadratic function of the DoC for the DoC > 0.82. They found that process-induced residual stresses cause out-of-plane deformations that resulted in asymmetric laminates being curved. They[18] conducted a parametric study for thin asymmetric laminates to investigate effects of cure cycle parameters on the process induced curvature and transverse mechanical properties and concluded that the curvature (and hence residual stresses) can be reduced without compromising the transverse mechanical properties by curing the laminate at a lower temperature for a longer period of time in two-stage cure cycles. In order to maintain transverse properties while modifying the cure cycle parameters to reduce the process induced curvature, the final DoC at any point of the laminate was not allowed to be less than 0.95. The optimal cure cycle thus found gave the final minimum DoC of 0.98 and reduced the non-dimensional curvature by 18% but increased the total cycle time by 3 h in comparison to the MRCC. However, introducing an intermediate low temperature dwell in the optimized cure cycle (thus converting the two-stage cycle to a three-stage cycle) reduced the curvature by 20% from that induced in the laminate cured with the two-stage MRCC without further lengthening the total cycle time.

By employing the cure kinetics model and material parameters used in White and Hahn's work,[18] Gopal et al.[19] determined an optimal cure cycle to minimize residual stresses in asymmetric $\left[0^{\circ}_{N}/90^{\circ}_{N}\right]$ cross-ply composite laminates. By considering one input variable at a time, they investigated effects of rates of the first-stage heating, the second-stage heating and the cooling on residual stresses, determined the optimal value for the three parameters which corresponds to the minimum in-plane axial stresses, and found an optimal cycle as a combination of these parameters with the assumption that there is no interaction among effects of these parameters. Temperatures and dwell times of the first- and the second-stage cure were not considered as variables in their study.

Using a design sensitivity analysis, Li et al.[20] determined a cure cycle for thick laminates which minimizes the cure time and keeps the maximum temperature in the laminate produced by the exotherm below an allowable value. Pantelelis et al.[21] used a genetic algorithm (GA) in conjunction with a 1D process model to obtain optimal cure cycle parameters for thermoset-matrix composites that reduce the cure time and satisfy the constraints on the minimum DoC and the maximum temperature in the laminate. Using dynamic artificial neural networks, Jahromi et al.[22] found cure cycle parameters to minimize the temperature gradients, maximize the final DoC and satisfy the constraint on the maximum allowable temperature. Using a coupled FEM and GA technique, Vafayan et al.[23] determined the optimal cure cycle parameters for a glass/epoxy laminate that minimize the cure time, gradients of the temperature and the DoC in the laminate as well as satisfy the constraint on the minimum DoC and the maximum allowable temperature. Pillai et al.[24] and Rai and Pitchumani[25] studied optimization problems of finding cure cycle parameters that reduce the total cycle time subjected to a set of constraints.

In this work, we numerically analyze curing of thermoset-matrix composites with functionalities built in the commercial software COMPRO for modeling the cure process, the finite element (FE) software ABAQUS for obtaining numerical solutions of the corresponding IBVPs and MATLAB for the GA. The cure model incorporated in COMPRO uses an integrated submodel approach similar to that of Loos and Springer[5] for simulating the cure process. The objective of the present study is to determine optimal parameters of the cure cycle that provide uniform and nearly complete curing of the laminate in the minimum time and simultaneously minimize the process induced residual stresses without adversely affecting the effective transverse modulus of the laminate. We use a GA with the Latin hypercube sampling (LHS) technique for the optimization study.

The rest of the manuscript is organized as follows. A brief description of the cure simulation model built in COMPRO is provided in the following section. Next, the efficacy of the simulation model is verified by comparing predictions from it with either experimental or numerical results available in the literature for two example problems. Then, the optimization problem is formulated and results are discussed. Conclusions of the work are summarized in the final section.

Simulation approach

The curing of a fiber-reinforced laminate, development of residual stresses in it and the prediction of elastic moduli of the cured laminate are studied by using the commercial FE software, ABAQUS, with the commercial software, COMPRO. The software COMPRO has built-in cure models and is coupled with ABAQUS to obtain numerical solutions of the IBVPs.

The ABAQUS-COMPRO combination simulates the cure process in three sequential steps, namely, thermo-chemical, flow-compaction and stress-deformation analyses. The three sub-models are one-way coupled in the sense that results from the thermo-chemical analysis are employed in the flow-compaction sub-model, and those from these two sub-models in the stress-deformation sub-model. In these analyses, it is assumed that the laminate is void-free, its plies are perfectly bonded and the material of each ply is homogeneous and transversely isotropic with the fiber axis as the axis of transverse isotropy. The effective thermo-mechanical properties are computed by using a micro-mechanics approach from those of the fibers and the matrix and their volume fractions.

The thermo-chemical model considers heat transfer among the air/fluid in the autoclave, the laminate and the tool, accounts for the heat generated/absorbed in the laminate due to exothermic/endothermic chemical reactions during the cure process, and predicts time histories of the temperature and the DoC at every point of the laminate. The inputs to the thermo-chemical model are values of the mass density, the specific heat and the thermal conductivity of constituents, the resin heat of reaction and an experimentally deduced expression for the rate of the DoC in terms of the temperature and the DoC.

The flow-compaction analysis utilizes results from the thermo-chemical model to simulate compaction of the laminate and the resin flow under the applied pressure. The laminate is idealized as a system of homogeneous, transversely isotropic and linearly elastic fiber-bed fully saturated with the resin. This analysis computes the fiber-bed displacements and the resin pressure from which other parameters such as the final thickness of the laminate, the fiber and the resin volume fractions, and the resin velocity are computed. The inputs to the flow-compaction model are values of permeabilities, elastic constants of the fiber-bed and the resin viscosity as a function of the temperature and the DoC. Here, values of the temperature and the DoC at a given time are obtained from the thermo-chemical analysis.

The stress-deformation model computes residual stresses and strains developed in the laminate. Since the material of each ply is assumed to be homogeneous, only residual stresses in a ply and not in a constituent are predicted. The inputs to this model are values of the elastic moduli and coefficients of thermal expansion of the fibers and the matrix, the specific volume shrinkage of the resin and the experimentally determined relation between the cure shrinkage and the resin volumetric strain. Since the resin elastic modulus is specified as a function of the DoC, its value at a material point is updated after every time step. The thermo-physical properties of the fibers are assumed to be independent of the cure process. The volume fractions of the fiber and the resin predicted from the flow-compaction analysis are used in the micro-mechanics equations to compute effective properties of the lamina.

The governing equations with pertinent initial and boundary conditions for the three sub-models and the micro-mechanics equations to compute effective properties of the composite ply are given in Johnston[26] and Hubert.[27]

Comparison of the presently computed results with those from the literature

We use the following error norm

$$\|e\|_0 = \left[\int_{d_0}^{d_1} [\psi_{\mathrm{Ref}}(s) - \psi_{\mathrm{Present}}(s)]^2 \mathrm{d}s \bigg/ \int_{d_0}^{d_1} \psi_{\mathrm{Ref}}^2(s) \mathrm{d}s \right]^{1/2} \tag{1}$$

to quantify the difference between the presently computed solutions for two example problems and their either numerical or experimental results available in the literature. In equation (1), d_0 and d_1 are either two instants of time or two points in space, and ψ_{Ref} (ψ_{Present}) the literature's (presently computed) solution.

We have depicted in Figure 1 the rectangular Cartesian coordinate system (x, y, z) and an N-layered pre-preg stack of length, width and thickness equal to a, b and H, respectively, with the thickness of each ply equaling H/N. Thus, $x = 0$ and a, and $y = 0$ and b represent edge surfaces of the laminate, and $z = H/2$ the mid-surface.

400-Ply 0° graphite/epoxy composite laminate

The first example problem, taken from Costa and Sousa[4] and Carlone and Palazzo,[28] involves curing of a $305 \times 254 \times 36.5$ mm graphite/epoxy composite laminate made of 400 plies of equal thickness with fibers in each layer oriented along the x-axis and the fiber volume fraction, $V_f = 0.58$. We use the cure-kinetic and the viscosity models for the epoxy resin, the material and the physical properties of the constituents (see the Appendix, subsection "Properties of graphite/epoxy composite"), the cure cycle and initial and boundary conditions the same as those used in Costa and Sousa[4] and Carlone and Palazzo.[28] In Figure 2, we have depicted time histories of the autoclave air temperature, T'(t), and the compaction pressure, P'(t), with their scales shown on the left and the right vertical axes, respectively.

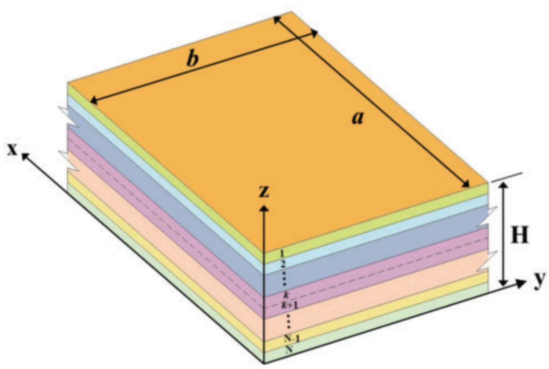

Figure 1. The geometry of the pre-preg stack and the coordinate system used in the analysis.

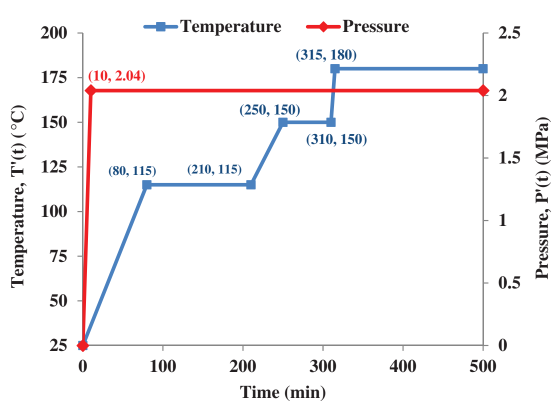

Figure 2. The cure temperature and pressure time histories taken from Costa and Sousa[4] and Carlone and Palazzo.[28]

Thermal histories. The temperature at all surfaces of the laminate is assumed to equal that of the surrounding air; thus, effects of the convection and thermal resistances associated with the bagging materials are neglected.[4] At time $t = 0$, it is assumed that the laminate is at 25°C with the DoC = 0 at every point.

In Figure 3(a) and (b), we have portrayed the presently computed time histories of the temperature and the DoC at centroids of the top and the middle surfaces of the laminate and those given in Costa and Sousa[4] and Carlone and Palazzo.[28] We note that the iterative scheme[26] employed in the current work assumes that in each time step either the temperature or the DoC is known and the other variable is found until its values at every point have converged within the prescribed tolerance of 0.1%. Based on the number of iterations required to obtain a converged solution, the size of the next time step is varied between the assigned minimum and maximum values, Δt_{min} and Δt_{max}, respectively. In Figure 3, we have compared solutions computed with $(N_x \times N_y \times N_z,\ \Delta t_{max},\ \Delta t_{min}) = (24 \times 18 \times 6,\ 60\,s,\ 0.01\,s)$ and $(30 \times 24 \times 8,\ 30\,s,\ 0.01\,s)$ where N_x, N_y and N_z denote, respectively, the number of 3D eight-node brick elements in the x-, the y- and the z-directions. With the minimum time step size of 0.01 s, a converged solution is computed. Results of Costa and Sousa[4] and Carlone and Palazzo[28] are also converged solutions with respect to the domain discretization. The two

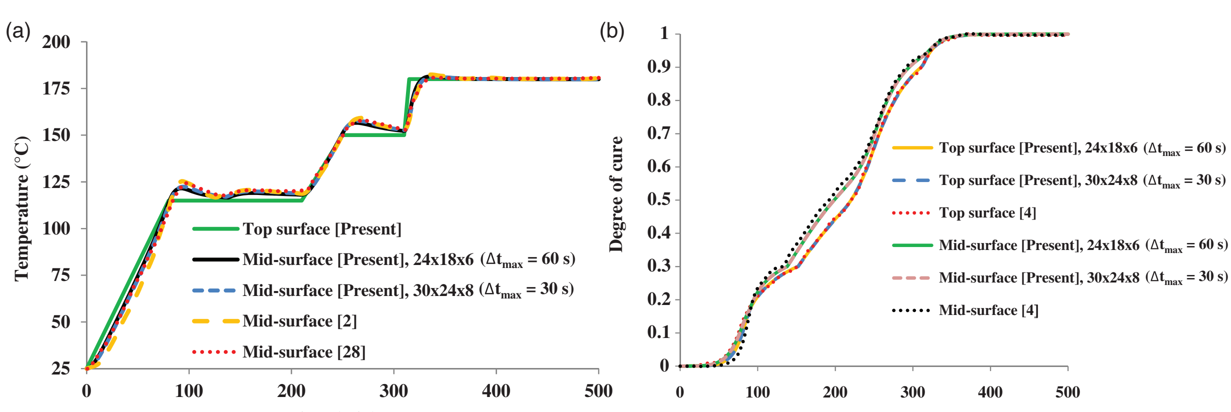

Figure 3. Comparison of the time histories of the (a) temperature and (b) DoC at centroids of the top- and the mid-surfaces of the laminate with those of Costa and Sousa[4] and Carlone and Palazzo.[28] The dotted curves are plotted using the data digitized from the plots of Costa and Sousa[4] and Carlone and Palazzo.[28]

sets of results for the temperature and the DoC are found to be very close to each other with $\|e\|_0$ less than 1.6% and 3.4% for the temperature and the DoC, respectively. A sharp increase in the DoC rate (measured by the slope of the curve in Figure 3(b)) at the start of the first two dwell periods is observed that causes the temperature inside the laminate becoming higher than the air temperature in the autoclave. There is a small difference between temperatures at the mid- and the top-surfaces for all times during the cure cycle. For $t < 80$ min, the temperature at the top surface is a little higher than that at the mid-surface, but the reverse holds for $80 < t < 210$ min and $250 < t < 310$ min suggesting that exothermic curing of the resin occurs during the time intervals for which the air temperature in the autoclave is kept constant.

Laminate compaction. The surface traction equal to the compaction pressure, P'(t), is prescribed on the top surface of the laminate, displacements at the bottom surface of the laminate are assumed to be zero and the normal displacement and the tangential tractions are assumed to be zero on the remaining four edge surfaces. The resin is allowed to flow out of the laminate only from the top surface and the resin flux (i.e., velocity normal to the surface) is taken to be zero at the remaining surfaces. It is equivalent to assuming that the bottom surface of the laminate is perfectly bonded to the impermeable, smooth and rigid tool, and stationary, impermeable and rigid walls touch the four-edge surfaces of the laminate. At time $t = 0$, displacements and the resin pressure in the uncured laminate are assumed to be zero.

In Figure 4, we have exhibited time histories of the converged values of the thickness reduction and the fiber volume fraction, V_f, during the consolidation process with their scales given on the left and the right vertical axes, respectively. The 23.6% and 22.7% reductions in the final laminate thickness, respectively, predicted by the present analysis and that reported in Costa and Sousa[4] differ from each other by 4%. We note that Costa and Sousa[4] assumed that the compaction pressure is applied at $t = 0$ while we have considered a rise time of 10 min before the compaction pressure becomes steady. As the compaction progresses, the resin flows out of the laminate and hence V_f increases. The value of V_f at the centroid of the laminate mid-surface increases from 0.58 at $t = 0$ to 0.715 at the end of the consolidation process, it is found to be constant through the laminate thickness, and the maximum variation in values of V_f in the xy-plane of the laminate is only 0.8%.

Good agreement between presently computed results and the numerical results of Costa and Sousa[4] and Carlone and Palazzo[28] who developed their own algorithms, observed from plots of Figures 3 and 4, verifies the correct implementation of the cure model in the commercial software, COMPRO, used in this work.

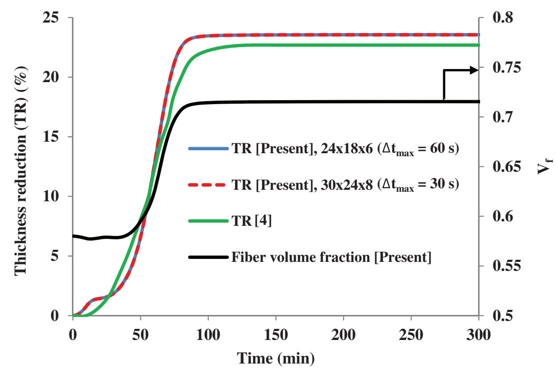

Figure 4. Time histories of the percentage reduction in the laminate thickness and the fiber volume fraction at the laminate centroid during the consolidation process. The green curve is plotted using the data digitized from the plot in Costa and Sousa.[4]

$[0^\circ_4/90^\circ_4]$ *Graphite/epoxy composite laminate*

The second example problem, taken from Kim and Hahn,[29] involves curing of a $152 \times 25 \times 1.2$ mm graphite/epoxy $[0^\circ_4/90^\circ_4]$ cross-ply laminate with $V_f = 0.6$. Thus, fibers in the top four and the bottom four layers are parallel to the x- and the y-axis, respectively. We note that Kim and Hahn[29] numerically performed thermo-chemical analysis and experimentally computed the transverse modulus of the lamina.

Thermal histories. For the thermo-chemical analysis, we use the cure-kinetics model, values of thermal and physical properties of the constituents (see Appendix, subsection "Properties of graphite/epoxy composite") and initial and boundary conditions the same as those used by Kim and Hahn.[29] The temperature at all surfaces of the laminate is assumed to equal that of the surrounding air, T'(t), whose time history is depicted in Figure 5. At time $t = 0$, it is assumed that the laminate is at 23°C and is uncured.

In Figure 6, we have portrayed time histories of the maximum and the minimum temperature, $T_{max}(t)$ and $T_{min}(t)$, and of the maximum and the minimum DoC, $c_{max}(t)$ and $c_{min}(t)$, in the laminate. Here, $\phi_{max\ (min)}(t) = \max\ (\min)\ \{\phi\ (x, y, z, t), (x, y, z) \in [0, a] \times [0, b] \times [0, H]\}$ with $\phi = T$ and c. These results suggest that the temperature and the DoC are essentially uniform in the laminate. Moreover, the final value of the DoC is 1 implying that the laminate is fully cured. We have also plotted in Figure 6 the numerical solution of Kim and Hahn[29] for the DoC time history (they found

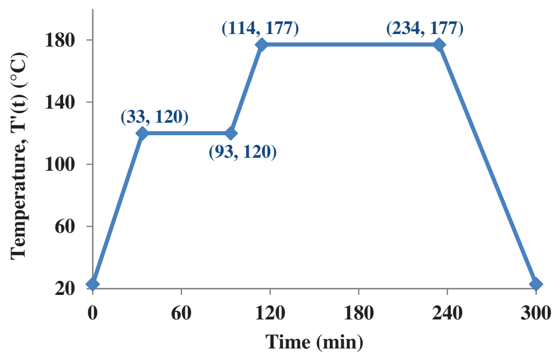

Figure 5. The autoclave temperature time history, taken from Kim and Hahn,[29] for the problem studied in subsections "Thermal histories" through "Residual stresses."

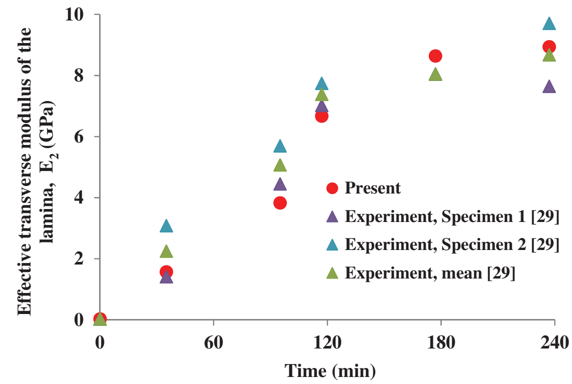

Figure 7. Time histories of the effective transverse modulus of the lamina. The plotted experimental data are digitized from the curve in Kim and Hahn.[29]

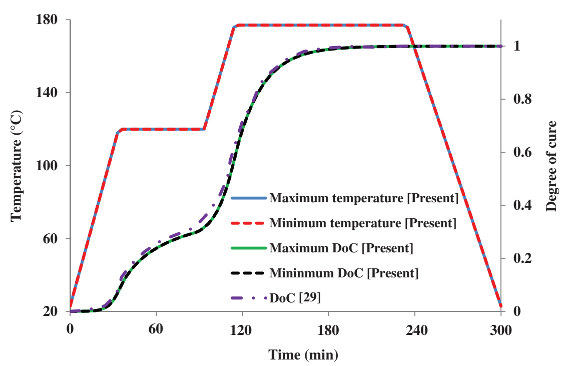

Figure 6. Time histories of the maximum and the minimum temperature and DoC in the laminate. The curve indicated as "DoC" is plotted using the data digitized from the corresponding plot in Kim and Hahn.[29]

it to be the same everywhere in the laminate) that differs from the present values by $\|e\|_0 = 3.6\%$. Kim and Hahn[29] did not provide the FE mesh used. The present converged solution is obtained with a uniform FE mesh of $150 \times 25 \times 6$ eight-node brick elements and $(\Delta t_{min}, \Delta t_{max}) = (0.01, 10)$ s.

Elastic moduli. In Figure 7, we have displayed evolution of the computed effective modulus, E_2, of the lamina in the direction transverse to the fibers and the corresponding two independent sets of experimental results.[29] In Kim and Hahn,[29] two $152 \times 25 \times 1.2$ mm $[90^\circ_8]$ panels were fabricated and their transverse elastic modulus found from the tensile test data. For each specimen, the cure was interrupted at t = 35, 95, 117, 177 and 237 min, the specimen was cooled to the room temperature at approximately 3°C/min and the specimens were tested. In our numerical simulations, we cool down the specimen to the room temperature and find the corresponding DoC, compute the resin modulus from the value of the DoC using the relation given in Table 8 and determine E_2 of the lamina using the micro-mechanics equation given in Johnston.[26] Thus, we perform five independent numerical simulations to compute E_2 at the five time instances. The presently computed effective transverse modulus is close to the experimental value. The value of E_2 of the cured lamina, 8.94 GPa, computed from the present analysis is only 3% larger than the mean of the elastic moduli, 8.67 GPa, of the two specimens found from the test data. The longitudinal modulus, E_1, of the lamina (computed using the micro-mechanics equation[26]), about 125 GPa, remains constant during the cure process since it is not a resin dominant property. With respect to the material principal axes (y_1, y_2, y_3) with the y_1- and the y_2-axes being parallel and transverse to the fiber direction and the y_3-axis along the thickness direction, the remaining effective elastic constants of the lamina computed using the corresponding micro-mechanics equations given in Johnston[26] are: $(E_3, G_{12}, G_{13}, G_{23}, \nu_{12}, \nu_{13}, \nu_{23}) = (8.94\,\text{GPa}, 4.36\,\text{GPa}, 4.36\,\text{GPa}, 3.03\,\text{GPa}, 0.25, 0.25, 0.44)$. At time t = 0, E_2 of the lamina equals 26 MPa. Knowing effective elastic constants of the laminas, those of the laminate can be computed using equations given by either Sun and Li[30] or Bogetti et al.[31] which for the $[0^\circ_4/90^\circ_4]$ laminate in the global (x, y, z) coordinate system are found to be $(E_x, E_y, E_z) = (67.22, 67.22, 10.63)$ GPa, $(G_{xy}, G_{xz}, G_{yz}) = (4.36, 3.57, 3.57)$ GPa and $(\nu_{xy}, \nu_{xz}, \nu_{yz}) = (0.03, 0.39, 0.39)$. Similarly, effective coefficients of thermal expansion and thermal conductivities of the lamina[26] with respect to the material principal axes, respectively, are $(\alpha_{11}, \alpha_{22}, \alpha_{33}) = (-2.58 \times 10^{-7}, 3.54 \times 10^{-5}, 3.54 \times 10^{-5})°C^{-1}$ and $(K_{11}, K_{22}, K_{33}) = (15.67, 0.53, 0.53)$ W/m-K. These properties for the laminate in the global (x, y, z) coordinate system computed using equations given in Bogetti et al.[31] and Johnston[26] are

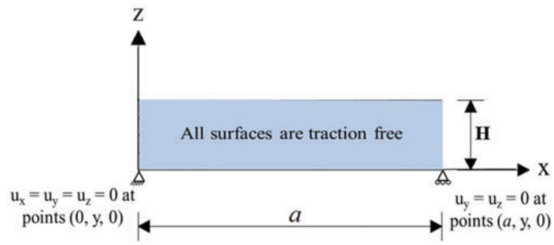

Figure 8. Boundary conditions used for the stress-deformation analysis for the problem studied in the section "Residual stresses."

$(\alpha_{xx}, \alpha_{yy}, \alpha_{zz}, \alpha_{xy}, \alpha_{xz}, \alpha_{yz}) = (2.63 \times 10^{-6}, 2.63 \times 10^{-6}, 4.89 \times 10^{-5}, 0, 0, 0)°C^{-1}$ and $(K_{xx}, K_{yy}, K_{zz}, K_{xy}, K_{xz}, K_{yz}) = (8.1, 8.1, 0.53, 0, 0, 0)$ W/m-K.

Residual stresses. In the absence of details of the experimental set-up used in Kim and Hahn's work,[29] we specify boundary conditions (BCs) shown in Figure 8 on the laminate boundaries for the stress-deformation analysis. All bounding surfaces of the laminate are assumed to be traction-free. The three displacements (u_x, u_y, u_z) of points located on the intersection of the bottom surface and the surface x = 0, i.e., points (0, y, 0), are assumed to be zero and displacements (u_y, u_z) in the y- and the z-directions of points located on the intersection of the bottom surface and the surface x = a, i.e., points (a, y, 0), are assumed to be zero. At time t = 0, it is assumed that the laminate is at 23°C, at rest, and is stress-free.

We have depicted in Figure 9 through-the-thickness distributions of the in-plane axial residual stresses, $(\sigma_{xx}, \sigma_{yy})$, along the transverse normal passing through the centroid of the laminate. The distributions of σ_{xx} and σ_{yy} are mirror images of each other about the mid-surface because of the 0° and 90° fibers below and above it. The maximum magnitude of σ_{xx} equals 0.056% of E_x. These residual stresses cause the laminate to deform into a doubly curved panel with approximately equal and opposite curvatures induced in the xz- and the yz-planes; these are depicted in Figure 10(a) and (b), respectively. The magnitude of the curvature in the xz- plane, χ_x, computed using equation (2)

$$\chi_x = 2h/(l^2/4 + h^2) \tag{2}$$

from the geometry of the deformed shape equals 3.65 m^{-1}. Here l and h are, respectively, the cord length and the laminate rise shown in Figure 10(a). Similarly, the magnitude of the curvature in the yz- plane, χ_y, equals 3.67 m^{-1}. Since the panel length in the y-direction is considerably less than that in the x-direction ($b = a/6$), the deformed cross-section of the panel in the yz-plane looks flat even though the radii of curvature in both planes are nearly the same.

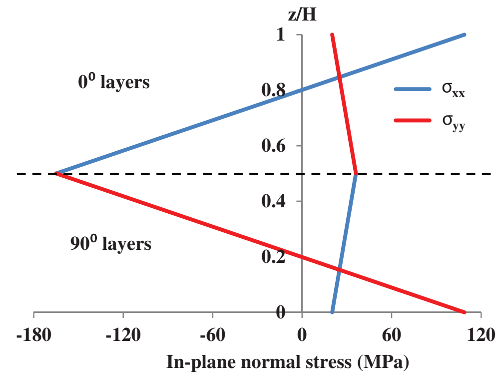

Figure 9. Through-the-thickness distributions of the in-plane axial residual stresses, σ_{xx} and σ_{yy}, at $(a/2, b/2, z)$ developed in the laminate at the end of the cure process.

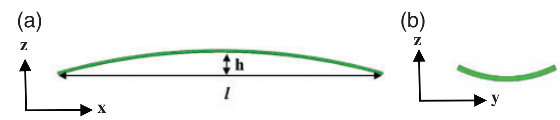

Figure 10. Deformed shapes of the cross-sections (a) y = b/2 (not to scale), and (b) x = a/2. Deformations are magnified by a factor of 10.

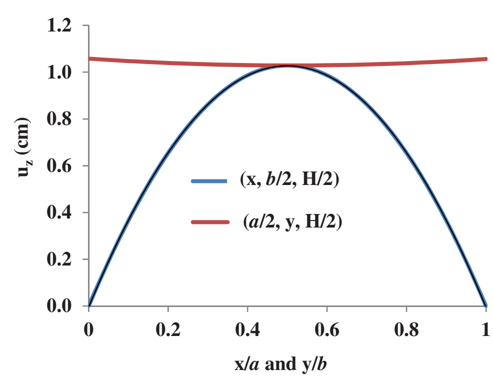

Figure 11. Variations of the transverse displacement, u_z, along the lines y = b/2 and x = a/2 on the mid-plane of the laminate.

In Figure 11, we have depicted the variation of the transverse displacement, u_z, along the lines, y = b/2 and x = a/2. The second-order polynomials fitted through (u_z, x) and (u_z, y) points by the least squares method with $R^2 = 1$ are $u_z = (-1.83x^2 + 0.275x)$ m and $u_z = (1.84y^2 - 0.0461y + 0.0108)$m which give the curvatures, $\chi_x = -\frac{\partial^2 u_z}{\partial x^2} = 3.66\,\text{m}^{-1}$ and $\chi_y = -\frac{\partial^2 u_z}{\partial y^2} = 3.68\,\text{m}^{-1}$. These values of χ_x and χ_y differ only by 0.3% from their corresponding magnitudes computed using equation (2).

Comparison of the experimental and the computed process induced curvatures. We now analyze curing of the

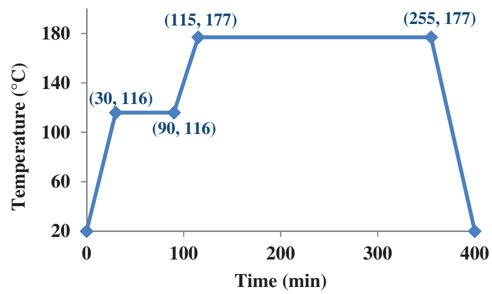

Figure 12. The cure temperature time history taken from Madhukar.[32]

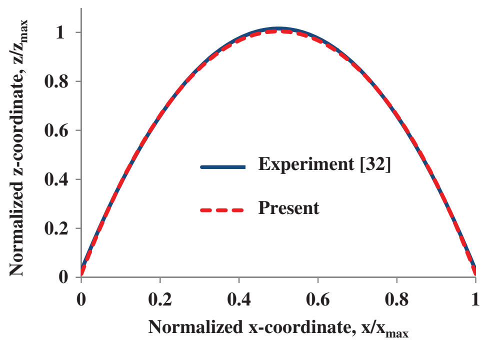

Figure 13. Final (deformed) shape of the line $y = b/2$ on the mid-surface of the cured laminate. The x- and the z-coordinates are normalized to take values between 0 and 1. The plotted experimental data are digitized from the photograph in Madhukar.[32]

laminate with $a = 254\,\text{mm}$, $b = 25.4\,\text{mm}$ and $\text{H} = 1.2\,\text{mm}$ that has been experimentally studied by Madhukar[32] using the cure temperature cycle depicted in Figure 12. The computed and the experimental final shapes of the cured laminate, depicted in Figure 13, are identical to each other, with the computed non-dimensional curvature, $\bar{\chi} = \chi\, H = 42.48 \times 10^{-4}$, differing by 1.9% from the experimental value, $\bar{\chi} = 42 \times 10^{-4}$ (mean of six test results).

Effects of heat convection and compaction pressure. In order to analyze effects of the heat convection and the consolidation pressure, we restudy the problem analyzed in subsections "Thermal histories" through "Residual stresses" but now assume that for all surfaces of the laminate the convection heat transfer coefficient, $h_c = 30$ and $10\,\text{W/m}^2\cdot\text{K}$, and the compaction pressure, $P'(t)$, is given by equation (3).

$$P'(t) = \begin{cases} 0.07t\,\text{MPa}, & 0 \le t \le 10\ \text{min} \\ 0.7\,\text{MPa}, & 10 \le t \le 290\ \text{min} \\ 0.7 - 0.07(t - 290)\,\text{MPa}, & 290 \le t \le 300\ \text{min} \end{cases} \tag{3}$$

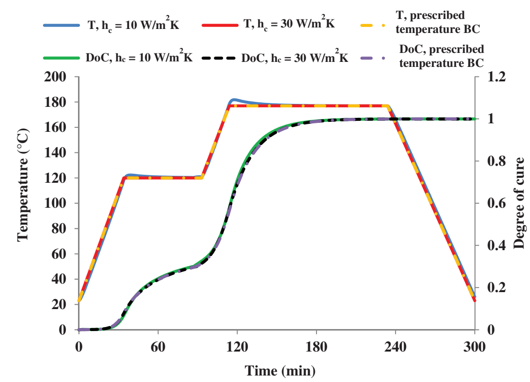

Figure 14. Time histories of the temperature and the DoC of the laminate for the problem studied in subsection "Effects of heat convection and compaction pressure."

In Figure 14, we have depicted time histories of the temperature and the DoC at the centroid of the laminate mid-surface for the prescribed temperature BCs, i.e., temperature equal to the air temperature, and $h_c = 30$ and $10\,\text{W/m}^2\cdot\text{K}$. For the three cases, the temperature and the DoC time histories at all points in the laminate are found to be essentially identical as indicated by nearly the same values of ϕ_{max} and ϕ_{min} ($\phi = \text{T}$ and c) in the laminate. The temperature and the DoC time histories for the prescribed temperature BC and the convective heat transfer boundary condition using $h_c = 30\,\text{W/m}^2\cdot\text{K}$ are identical. For $h_c = 10\,\text{W/m}^2\cdot\text{K}$, slight temperature overshoots are observed at the start of the two dwell periods and the DoC time history differs from that for the prescribed temperature BC by $\|e\|_0 = 1\%$. However, the final value of the DoC = 1 for the three cases.

The curvatures induced in the laminate for $h_c = 30$ and $10\,\text{W/m}^2\cdot\text{K}$ and subjected to the compaction pressure given by equation (3) are found to be $\bar{\chi} = 43.82$ and 43.43, respectively, which differ from 43.79 for the prescribed temperature BC and no compaction pressure by 0.07% and 0.8% only. Thus, for the problem studied, consideration of heat convection and the compaction pressure has negligible effects on the output parameters.

Cure cycle optimization

We now optimize the curing process for the graphite/epoxy $[0^{\circ}_4/90^{\circ}_4]$ composite panel, analyzed in subsection "$[0^{\circ}_4/90^{\circ}_4]$ graphite/epoxy composite laminate", for which the computed results agreed well with the experimental findings.[29,32] We take values of all parameters to be the same as those used in subsection "$[0^{\circ}_4/90^{\circ}_4]$ graphite/epoxy composite laminate", neglect effects of the compaction pressure and consider convective heat transfer with $h_c = 30\,\text{W/m}^2\cdot\text{K}$ for all surfaces of the laminate. We first identify the output parameters to be optimized, constraint conditions and the cure cycle variables. Next, we deduce by using the LHS method, response functions relating each output parameter to the input variables. Finally, we formulate the optimization problem and solve it using a GA.

Identification of output parameters

The goal is to optimize parameters of the cure cycle depicted in Figure 5 in order to (i) minimize the process induced curvature in the laminate, (ii) minimize the total cycle time, t_{cycle}, (iii) maximize the effective transverse modulus of the lamina, E_2, and (iv) achieve complete and uniform curing of the laminate, i.e., obtain the DoC, $c = 1$, at every point in the laminate.

We recall that the effective transverse modulus, E_2, of the lamina is computed using the micro-mechanics equation[26] from the moduli of the fibers and the matrix and their volume fractions. Since the resin modulus varies with the DoC (see Table 8), E_2 is a function of the DoC, c. The variation of E_2 with c, displayed in Figure 15, reveals that E_2 is a monotonically increasing function of c. Thus, the maximum value, 8.94 GPa, of E_2 is obtained for $c = 1$. Hence, by requiring that $c = 1$ at every point in the laminate, we ensure that E_2 is maximum. We note that the effective moduli of the laminate, $(E_x, E_y, E_z) = (67.22, 67.22, 10.63)$ GPa, are also maximum when E_2 has the maximum value of 8.94 GPa. Thus, objectives of the optimization problem are to minimize the non-dimensional curvature, $\bar{\chi}$, and the total cycle time, t_{cycle}, and obtain $c = 1$ everywhere in the laminate.

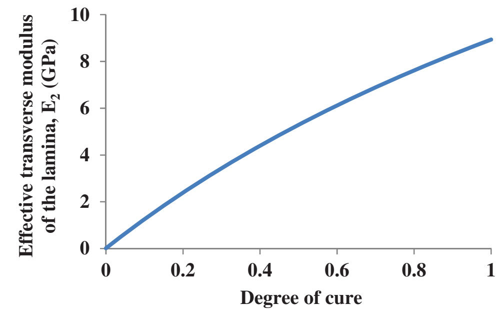

Figure 15. Variation of the effective transverse modulus of the lamina with the DoC.

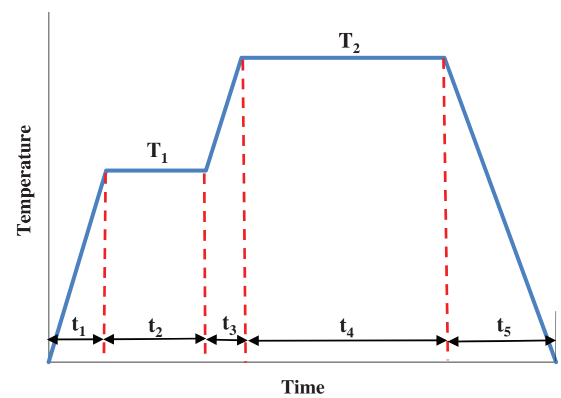

Figure 16. Schematic depiction of parameters of the cure temperature cycle.

Identification of input variables

We describe the cure cycle depicted in Figure 5 by seven input variables (T_1, T_2, $t_1, \ldots, t_5$), shown in Figure 16. The range of each variable, i.e., the design space, used in the optimization study is listed in Table 1.

Table 1. The range of cure cycle parameters used in the optimization study.

Parameter (units)	Symbol	Minimum value	Maximum value
T_1 (°C)	X_1	80	140
T_2 (°C)	X_2	145	215
t_1 (min)	X_3	5	60
t_2 (min)	X_4	10	120
t_3 (min)	X_5	5	60
t_4 (min)	X_6	10	240
t_5 (min)	X_7	5	60

Deduction of response functions

We normalize the seven input variables, X_i $(i = 1, 2, \ldots, 7)$, using equation (4) by their extreme values listed in Table 1. Thus, in the normalized space, $0 \leq \hat{X}_i \leq 1;\ \ i = 1,\ 2, \ldots, 7.$

$$\hat{X}_i = \frac{X_i - X_i^{min}}{X_i^{max} - X_i^{min}} \tag{4}$$

We generate random input vectors $(\hat{X}_1,\ \hat{X}_2,\ \ldots,\ \hat{X}_7)$ using the LHS technique[33,34] in conjunction with MATLAB. In the LHS technique, the number, n, of samples (experiments) to be constructed is predefined by the user and is independent of the number of input variables. The range of each input variable is divided into n segments of equal length. Thus, for constructing n samples of m input parameters, n points are randomly selected in the m-dimensional space to satisfy the Latin-hypercube requirement. Statistically, a square grid containing sample points in a 2D domain is a Latin square if and only if there is only one sample point in each row and column. A Latin-hypercube is a generalization of the Latin-square to m-dimensional space. In this study, $m = 7$, and we take $n = 120$ and 180. Thus, we perform two independent sets of 120 and 180 numerical experiments (simulations), and for each simulation, we compute values of c at every point in the laminate and the non-dimensional curvature, $\bar{\chi}$.

The computed maximum and minimum values, c_{max} and c_{min}, of the DoC are found to be essentially equal to each other implying that each cure cycle provides uniform final curing of the laminate.

We fit a complete polynomial of degree 2 using the least squares method to the ($\bar{\chi}$, $\hat{\mathbf{X}}$) and (c, $\hat{\mathbf{X}}$) data points. That is,

$$Y_i\left(\hat{\mathbf{X}}\right) = a_0^{(i)} + \sum_{k=1}^{7} a_k^{(i)} \hat{X}_k + \sum_{j=1}^{7}\sum_{m=j}^{7} a_{jm}^{(i)} \hat{X}_j \hat{X}_m \ (i = 1,\ 2) \tag{5}$$

where Y_1 and Y_2 are $\bar{\chi}$ and c, respectively, and values of the 36 coefficients in equation (5) for $n = 120$ and 180 for the two output functions are given in Table 9. The R^2 values of the fit for $\bar{\chi}$ and c obtained with $n = 120$ (180) are 0.96 (0.95) and 0.85 (0.85), respectively.

In order to verify the accuracy of model fits obtained from 120 and 180 simulations, we randomly generate 10 new samples of the normalized input vector, $\hat{\mathbf{X}}$, that are different from those used for deducing the model fits. This is ensured by having non-zero Euclidean distance of the new sample points from those used to find values of coefficients in equation (5). For these 10 samples, the % difference between the values of $\bar{\chi}$ and c from the model fits and the simulations are listed Table 2. The maximum difference of 4.7% (1.2%) for $n = 120$ (180) implies that formula (5), especially for $n = 180$, provides good estimates of $\bar{\chi}$ and c for all values of $\hat{\mathbf{X}}$.

Henceforth, we use equation (5) with coefficients derived from results of 180 simulations. Even though values of coefficients in equation (5) for $n = 120$ and 180 listed in Table 9 differ noticeably from each other, results predicted by the two fits are nearly the same as evidenced by values reported in Table 2.

Table 2. Difference (%) between the values obtained from simulations and those found from equation (5).

Sample	$n = 180$		$n = 120$	
	$\bar{\chi}$	c	$\bar{\chi}$	c
1	0.48	0.80	0.23	0.63
2	1.03	1.91	0.87	0.79
3	1.50	2.06	0.72	0.66
4	1.10	2.87	0.36	0.45
5	1.55	4.65	1.41	0.72
6	0.49	1.44	0.36	0.94
7	0.25	1.48	0.92	0.00
8	0.87	2.27	0.51	1.39
9	2.10	3.83	0.12	1.00
10	0.69	0.45	0.09	0.23
Maximum	2.10	4.65	1.41	1.39
Mean	1.00	2.18	0.56	0.68

Formulation of the optimization problem

The optimization problem reduces to finding the normalized vector of cure cycle variables, $\hat{\mathbf{X}}$ ($0 \leq \hat{X}_i \leq 1$; i = 1, 2,..., 7), that minimizes the non-dimensional curvature, $\bar{\chi}(\hat{\mathbf{X}})$, and the total cycle time, t_{cycle} ($\hat{\mathbf{X}}$), and satisfies the constraint, c ($\hat{\mathbf{X}}$) = 1 with $\bar{\chi}(\hat{\mathbf{X}})$ and c ($\hat{\mathbf{X}}$) given by equation (5), and

$$t_{cycle}\left(\hat{\mathbf{X}}\right) = \sum_{i=3}^{7}\left[X_i^{min} + \hat{X}_i\left(X_i^{max} - X_i^{min}\right)\right] \tag{6}$$

As mentioned in subsection "Identification of output parameters," the maximum value, 8.94 GPa, of E_2 for the lamina occurs when c = 1. This value is reduced by less than 3% (see Figure 15) for c = 0.96. Hence, rather than imposing the constraint c ($\hat{\mathbf{X}}$) = 1, we require that the minimum DoC in laminate must exceed a specified value, c', i.e., c ($\hat{\mathbf{X}}$) ≥ c', and analyze the problem for different values of c' ∈ [0.96, 1].

We recall that a multi-objective optimization problem may not have a unique solution but has a set of Pareto optimal solutions.[35] A Pareto optimal solution cannot be improved for an objective function without worsening the solution of at least one other objective function. In other words, while selecting one Pareto optimal solution over another to achieve gain in one objective function, there is always some sacrifice in at least one other objective function. Thus, it may be difficult to decide which Pareto optimal solution(s) to choose for a given problem. To overcome this, we convert the two-objective optimization problem into a single objective problem by moving the total cycle time to the set of constraints and require that it not exceed the allowable time, t', i.e., $t_{cycle}(\hat{\mathbf{X}})$ ≤ t', and analyze the problem for different values of t' ≤ 540 min. We note that the total cycle time for the maximum values listed in Table 1 of the input variables X_3 through X_7 does not exceed 540 min.

In order to solve the single objective optimization problem of finding the input vector $\hat{\mathbf{X}}^*$ in the solution space $0 \leq \hat{X}_i^* \leq 1$ (i = 1, 2,..., 7) so that $\bar{\chi}(\hat{\mathbf{X}}^*)$ is the minimum, c ($\hat{\mathbf{X}}^*$) ≥ c' and $t_{cycle}(\hat{\mathbf{X}}^*)$ ≤ t', we consider c' = 0.96, 0.98, 0.995 and t' = 120, 180,..., 540 min resulting in 24 cases for the optimization problem. We realize that the total cycle times t' = 120 and

180 min are very short. However, we use them to see how they affect output parameters of the cured laminate. We use a GA included in MATLAB to solve the optimization problem.

Brief description of GA. GAs are based on the concept that unfit species extinct and the strong ones pass their genes to future generations through reproduction. A typical GA has the following steps[36,37]:

(i) *Population initialization*. The algorithm begins by generating a random initial population which is a collection of solution vectors, called individuals, satisfying the constraints and the bounds on the variables.
(ii) *Computation of fitness scores*. The objective function is evaluated for each member of the current population, and its value is scaled to obtain the fitness score of the individual so that the individual with the lowest value of the objective function (the most fit) has the highest fitness score and that with the highest value of the objective function (the least fit) has the lowest score.
(iii) *Selection of parents*. A group of individuals, called parents, is selected from the current population for mating based on their fitness scores (individuals with higher fitness score have greater chance of being selected than those with lower fitness value).
(iv) *Generation of children*. The children are generated from parents by three methods, namely, elitism, crossover and mutation; these children replace the present population and form a new generation. The individuals in the current generation that have the best fitness scores are passed to the next generation without any alteration and are called elite children. The crossover children are generated by combining entries of the vectors, called genes, of a pair of parents whereas the mutation children are generated by making random changes to a single parent. The elitism ensures that the best solution(s) from a population is preserved and the algorithm does not regress. The crossover enables the algorithm to extract the best genes from individuals and combine them to produce children that are potentially superior to their parents. The mutation enhances the diversity of the population which in turn increases the chances of generating individuals with better fitness values.
(v) *Checking for stopping criteria*. The steps (ii) through (iv) are repeated until a prescribed stopping criterion has been met.

We use the Augmented Lagrangian GA[38,39] to solve the optimization problem with non-linear constraints that are satisfied within a tolerance of 10^{-6}. We employ a rank-based roulette wheel selection strategy[40] to select parents for mating in which the probability of an individual being selected depends upon its fitness rank relative to the entire population rather than the actual value of the objective function, thereby eliminating the effect of spread in values of the objective function. With n_p equaling the size of the population, and n_e, n_c and n_m the number of the elite, the crossover and the mutation children, respectively, in the population ($n_e + n_c + n_m = n_p$), we specify $n_e = 2$ and $n_c = C_f (n_p - n_e)$ with the crossover fraction, $C_f = 0.8$, following the MATLAB guidelines. We stop the algorithm when the average change in the best value of the objective function (corresponds to that of the fittest individual in a generation) for 50 consecutive generations is less than 10^{-10}.

Analysis of the optimization results

Effect of the algorithm variables on results. Before solving the optimization problem for 24 cases, for one case (c' = 0.995 and t' = 300 min) we analyze the effect on the best (minimum) value of the objective function (the non-dimensional curvature) of the (i) population size, n_p, (ii) number of elite individuals, n_e, in the population, and (iii) randomization of the initial population.

Variations of the best value of $\bar{\chi}$ with n_p and n_e depicted in Figure 17(a) and (b), respectively, reveal that optimal values of n_p and n_e are 500 and 2, respectively, although the best value of $\bar{\chi}$ varies by less than 1.2% over the ranges of n_p and n_e considered. Henceforth, we use $n_p = 500$ and $n_e = 2$.

The algorithm randomly generates the initial population and the final result may not be exactly the same if the same problem is resolved. Hence, we solved the same problem five times using the algorithm, and found the five results to be identical implying that the random generation of the initial population has no effect on the results.

Results for optimal cure cycles. The optimal cure cycles obtained from the algorithm for the 24 cases, i.e., for the three values of c' and the eight values of t', are depicted in Figures 18(a) to 18(c), and labeled as C1 through C24. The best values of $\bar{\chi}$ and of t_{cycle} satisfying the constraint $t_{cycle} \leq t'$ are listed in Table 3. The value reported in the column "Diff." is the relative difference between the values of $\bar{\chi}$ for the laminate cured with the optimal cycle and that with the MRCC. The final value of the DoC equals c' for all cases studied. We note that for $t_{cycle} = 300$ min of the MRCC, c = 1, $E_2 = 8.94$ GPa and $\bar{\chi} = 43.75$.

Results reported in Table 3 are depicted in Figure 19 as plots of $\bar{\chi}$ vs. t_{cycle} for the three values of c'; the filled black circle represents the value of $\bar{\chi}$ for the MRCC.

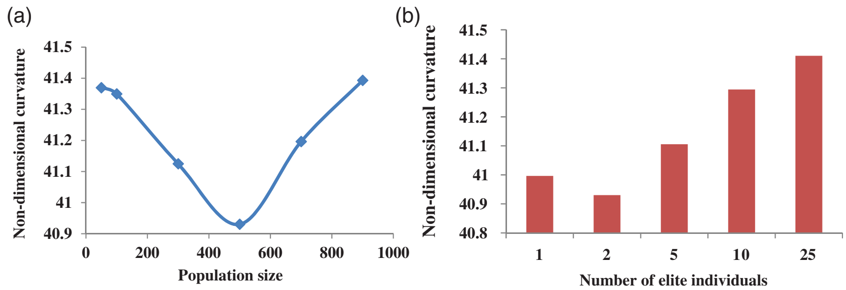

Figure 17. Variation of the best value of the non-dimensional curvature with the (a) population size and (b) number of elite individuals in the population.

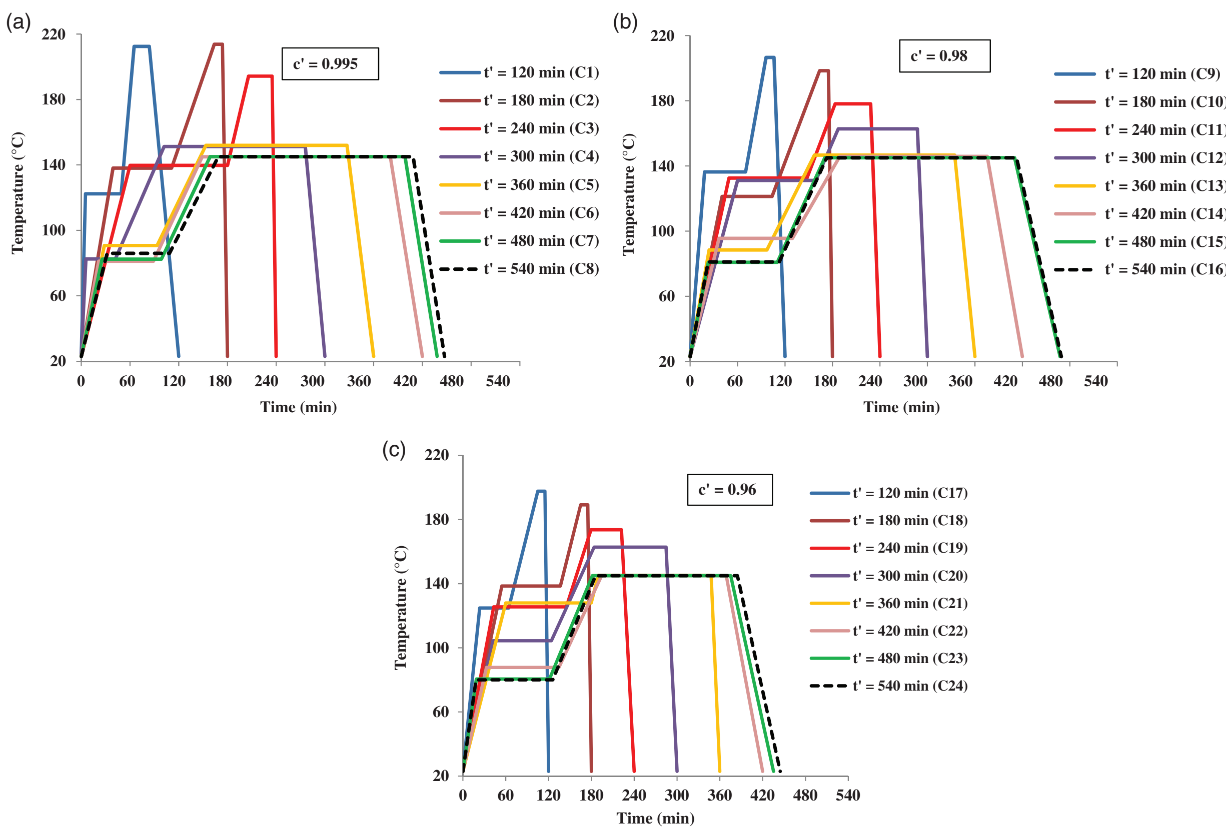

Figure 18. Optimal cure cycles satisfying the constraints: total cycle time, $t_{cycle} \leq t' = 120, 180, \ldots, 540$ and the degree of curve, $c \geq c'$ for (a) $c' = 0.995$, (b) $c' = 0.98$, and (c) $c' = 0.96$.

These results indicate that for a given prescribed lower limit of the DoC, the curvature induced in the laminate decreases with an increase in the overall cycle time. The cure cycles depicted in Figure 18 suggest that in order to obtain the prescribed minimum value of the DoC in less time, the laminate should be cured at higher temperatures T_1 and T_2. However, it increases the laminate curvature, $\bar{\chi}$, as evidenced by results listed in Table 3. In order to reduce $\bar{\chi}$ while maintaining the minimum prescribed value of the DoC, the laminate should be cured at lower temperatures T_1 and T_2 for a longer period of time resulting in larger values of the overall cycle time. These results agree with those of White and Hahn[19] who found that by decreasing the cure temperature T_2 from 182°C (which is in the MRCC) to 165°C and by increasing the corresponding dwell time from 4 to 7 h, the curvature induced in the BMI laminate is reduced by 18%, and the DoC of the laminate equaled 0.98.

The eight cure cycles for $c' = 0.995$ (C1 through C8) provide $E_2 = 8.9$ GPa which is only 0.35% less than its maximum value, 8.94 GPa, obtained with the MRCC. The cycle C1 cures the laminate in 120 min; however,

Table 3. The optimum value of the non-dimensional curvature obtained from the optimized cure cycles satisfying $t_{cycle} \leq t'$ and $c \geq c'$.

	c' = 0.995				c' = 0.98				c' = 0.96			
t' (min)	Cycle label	t_{cycle} (min)	$\bar{\chi}$	% Diff.	Cycle label	t_{cycle} (min)	$\bar{\chi}$	% Diff.	Cycle label	t_{cycle} (min)	$\bar{\chi}$	% Diff.
120	C1	120	47.43	8.41	C9	120	44.90	2.63	C17	120	43.44	−0.70
180	C2	180	42.98	−1.76	C10	180	42.29	−3.34	C18	180	41.28	−5.64
240	C3	240	41.47	−5.20	C11	240	41.39	−5.39	C19	240	40.61	−7.19
300	C4	300	40.93	−6.45	C12	300	40.56	−7.30	C20	300	40.43	−7.60
360	C5	360	40.40	−7.67	C13	360	39.44	−9.85	C21	360	38.64	−11.69
420	C6	420	39.70	−9.27	C14	420	39.25	−10.30	C22	420	38.38	−12.28
480	C7	438	39.66	−9.36	C15	468	38.96	−10.96	C23	435	38.28	−12.51
540	C8	447	39.65	−9.36	C16	469	38.96	−10.96	C24	445	38.28	−12.51

Note. Here t' is the maximum allowable cycle time and c' is the minimum desired DoC. For the MRCC, $\bar{\chi} = 43.75$, $t_{cycle} = 300$ min.

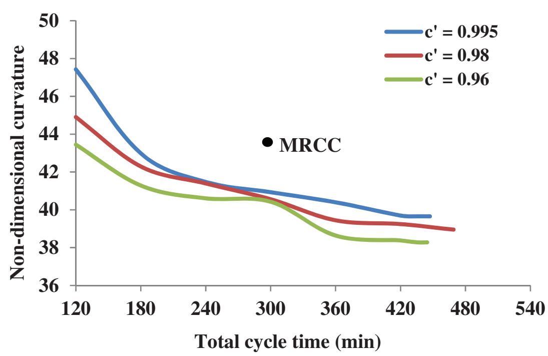

Figure 19. Variation of the non-dimensional curvature with the total cycle time.

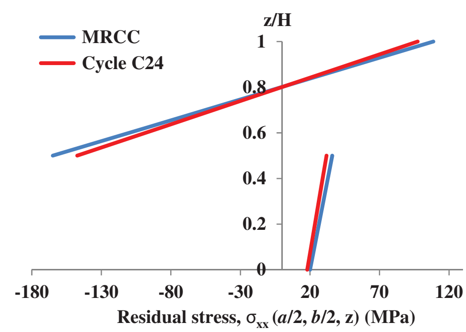

Figure 20. Through-the-thickness distributions of the residual stress, σ_{xx}, at (a/2, b/2, z) in the laminate cured with the MRCC and cycle C24.

it increases $\bar{\chi}$ by 8.4% over that for the MRCC. The total times of the cycle C4 and the MRCC are equal; however, $\bar{\chi}$ for the cycle C4 is 6.4% less than that for the MRCC. The curvature induced in the laminate cured with either cycle C7 or cycle C8 is 9.4% less than that for the MRCC, but these cycles require 50% more curing time.

The eight cure cycles for c' = 0.98 (C9 through C16) provide $E_2 = 8.81$ GPa which is 1.4% less than its maximum value. In comparison to the MRCC, cycles C10 and C11 save 2 h and 1 h, respectively, and reduce the curvature by 3.3% and 5.4%, respectively. Cycles C15 and C16 are identical to each other and reduce the curvature by 11% but require 56% more time than the MRCC.

The eight cure cycles (C17 through C24) for c' = 0.96 provide $E_2 = 8.68$ GPa which is 2.8% less than its maximum value. The $\bar{\chi}$ for cycle C17 is about the same as that for the MRCC, but it saves 3 out of 5 h of the curing time. The cycle C19 (C20) reduces $\bar{\chi}$ and the cure time by 7.2% (7.6%) and 1 (0) h, respectively. The cycles C23 and C24 are nearly the same and reduce $\bar{\chi}$ by 12.5% but increase the total cycle time by about 48% over that for the MRCC.

Recalling that solutions of the optimization problem are based on equation (5), we compare them with those obtained using the software ABAQUS coupled with COMPRO. For the 24 optimal curing cycles, results for c and $\bar{\chi}$ obtained from model fits and simulations are found to have the average difference of 1% and 0.6%, respectively, and for each cycle, $c_{max} = c_{min}$, i.e., the laminate is uniformly cured.

In Figure 20, we have compared through-the-thickness distributions of the in-plane axial residual stress, σ_{xx}, along the transverse normal passing through the laminate centroid cured with the MRCC and cycle C24. The maximum magnitude of the residual stress, σ_{xx}, for cycle C24 is less than that for the MRCC with the average difference $\|e\|_0 = 11\%$, which is close to the reduction in the curvature reported in Table 3. Thus, changes in the curvature, reported in Table 3, for optimal cure cycles are good indicators of the change in the residual stresses in comparison to those for the MRCC.

Optimal cure cycles for a thick laminate. We now study the optimization problem for the curing of the $[0^{\circ}_{N}/90^{\circ}_{N}]$ laminate studied above but change N from 4 to 40 which corresponds to the change in H from 1.2 to 12 mm. Through-the-thickness distributions of the residual stress, σ_{xx}, at points ($a/2$, $b/2$, z) for the two laminates cured with the MRCC depicted in Figure 21 reveal that the maximum magnitude of the residual stress induced in the 12-mm-thick laminate is about 7% more than that for the 1.2-mm-thick laminate. We note that the MRCCs for the two laminates are the same. Although not exhibited here, the through-the-thickness distribution of σ_{yy} is found to be the mirror image of that for σ_{xx} about the mid-surface for the two laminates. Moreover, σ_{xx} and σ_{yy} are found to be uniform in the xy-plane of the laminate except for points situated in the vicinity of the edges x = 0 and a distant from the edge by less than 5% of the edge-length. However, the maximum difference in magnitudes of σ_{xx} at two points in the xy-plane of the laminate is found to be at most 14% for the two laminates; this maximum difference occurs on the bottom surface of the laminate in the region $x/a \leq 0.05$. Furthermore, unlike the thin laminate, the thick laminate remains flat. Hence, rather than considering the non-dimensional curvature as the objective function, we take $\sigma_{xx}^{\max} = \max\left\{abs\,[\sigma_{xx}(a/2,\ b/2,\ z)],\ 0 \leq z \leq H\right\}$ as the objective function for the thick laminate and find the optimal cure cycle that minimizes $\sigma_{xx}^{\max}$, provides uniformly cured laminate, and satisfies constraints (i) c ≥ c' everywhere in the laminate, and (ii) $t_{cycle} \leq t'$.

Following the same procedure as that for the 1.2-mm-thick laminate and taking $n = 180$, values of the 36 coefficients in equation (5) are given in Table 10 with the R^2 values of the least squares fit for $\sigma_{xx}^{\max}$ and c_{min} equaling 0.94 and 0.83, respectively. It is found that, unlike for the thin laminate, all 180 cure cycles do not give uniform curing of the thick laminate and the maximum difference between the values of c_{max} and c_{min} equals 1.83%. Although this difference is small, for the optimization problem we specify the constraint $c_{min} \geq 0.995$, thereby ensuring the complete and the uniform curing of the laminate; the latter due to the reason that the maximum possible difference between c_{max} and c_{min} is negligible (≤0.5%). The other constraint is $t_{cycle} \leq t'$. We consider t' = 120, 180, and 240 min. These values of t' are smaller than the total cycle time, 300 min, for the MRCC.

We verify the accuracy of model fits given by equation (5) by comparing in Table 4 results for $\sigma_{xx}^{\max}$ and c_{min} obtained from the model fits with those computed from simulations for randomly generated 10 samples of $\hat{\mathbf{X}}$ that are different from those used for deducing the model fits. The results reported in Table 4 indicate that the maximum (mean) of 10 sets of results for differences between the values of $\sigma_{xx}^{\max}$ and c_{min} found from the simulations and equation (5) are 2.4% (1.1%) and 2.9% (0.9%), respectively, thereby implying that predictions from model fits are reasonably accurate.

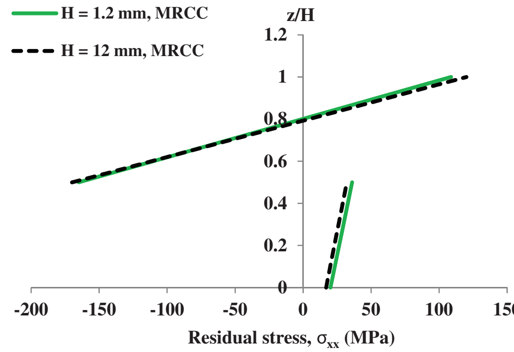

Figure 21. Through-the-thickness distributions of the residual stress, σ_{xx}, at ($a/2$, $b/2$, z) in the 1.2 - and the 12-mm-thick laminates cured with the MRCC.

Table 4. Percent difference between the values obtained from simulations and that found from equation (5).

Sample	$\sigma_{xx}^{\max}$	c_{min}
1	2.43	0.16
2	0.46	0.68
3	0.04	0.49
4	0.87	2.86
5	1.85	0.25
6	1.25	0.85
7	1.17	0.77
8	1.75	0.03
9	0.07	1.40
10	1.30	0.96
Maximum	2.43	2.86
Average	1.12	0.85

We have depicted in Figure 22 optimal cure cycles C25, C26 and C27 obtained for the 12-mm-thick laminate corresponding to the three values of t'.

The optimum values of the objective function, $\sigma_{xx}^{\max}$, for cycles C25, C26 and C27 are listed in Table 5. The column "Diff." has the % difference between values of $\sigma_{xx}^{\max}$ for the laminates cured with the optimal and the MRCC cycles with the latter equaling 169 MPa. The values of t_{cycle} and c_{min} for each of three cycles are equal to t' and 0.995, respectively. The effective

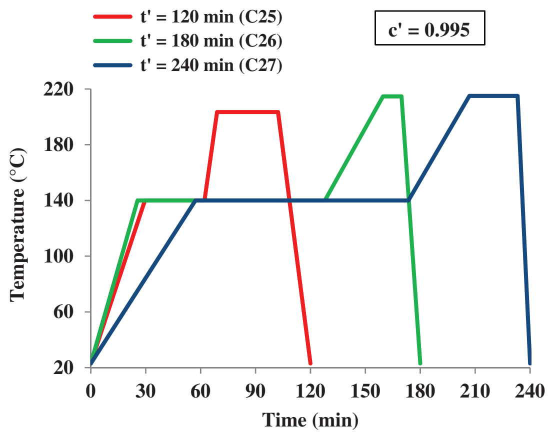

Figure 22. Optimal cure cycles for the 12-mm-thick laminate satisfying the constraints: total cycle time, $t_{cycle} \leq t' = 120$, 180 and 240 min and the minimum , $c_{min} \geq 0.995$

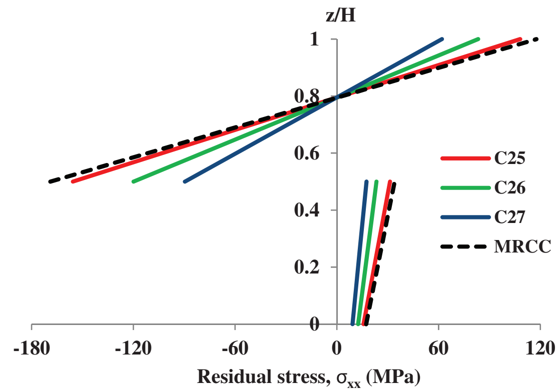

Figure 23. Through-the-thickness distributions of the residual stress, σ_{xx}, at (*a*/2, *b*/2, z) in 12 mm thick $[0^\circ_{40}/90^\circ_{40}]$ laminate cured with the MRCC, and optimal cycles C25, C26 and C27.

Table 5. The optimum value of σ_{xx}^{max} obtained from the optimized cure cycles satisfying $t_{cycle} \leq t'$ and $c_{min} \geq 0.995$.

t' (min)	Cycle label	σ_{xx}^{max}	% Diff.
120	C25	150.23	11.11
180	C26	112.46	33.46
240	C27	92.05	45.53

Note. Here, t' is the maximum allowable cycle time. For the MRCC, $\sigma_{xx}^{max} = 169$ MPa, $t_{cycle} = 300$ min.

transverse modulus of the lamina, E_2, achieved with the three cure cycles is 8.9 GPa which is only 0.35% less than its maximum value, 8.94 GPa, obtained with the MRCC. We note that the effective elastic moduli of the $[0^\circ_{40}/90^\circ_{40}]$ laminate, (E_x, E_y, E_z), computed using micromechanics equations[30,31] equal (67.22, 67.22, 10.63) corresponding to the maximum value of E_2, 8.94 GPa, of the lamina and are the same as those for the $[0^\circ_4/90^\circ_4]$ laminate. In comparison to the MRCC, cycles C25, C26 and C27 reduce σ_{xx}^{max} by 11%, 33% and 46%, respectively, and the total cycle time by 3, 2 and 1 h, respectively. Since solutions of the optimization problem are based on results predicted from model fits given by equation (5), we verify their accuracy by comparing values of c_{min} and σ_{xx}^{max} for the three cure cycles with those obtained from the simulations. The two sets of results are found to differ from each other at most by 0.5% and 6.2% for c_{min} and σ_{xx}^{max}, respectively.

We have compared in Figure 23 through-the-thickness distributions of the residual stress, σ_{xx}, at points (*a*/2, *b*/2, z) for the 12-mm-thick laminate cured with the MRCC and cycles C25, C26 and C27. The residual stresses, σ_{xx} for cycles C25, C26 and C27 are less than that for the MRCC by $\|e\|_0 = 8\%$, 28% and 47%, respectively.

Conclusions

The curing of fiber-reinforced composite laminates has been studied using a process model, and optimal cure cycles for asymmetric laminates have been found using a GA in conjunction with the LHS method. Equations governing the cure process are solved by using the finite element method in the space domain and the implicit backward Euler method in the time domain, and results are verified by comparing them with either experimental or numerical results available in the literature. All computations have been performed with commercial software COMPRO, ABAQUS and MATLAB with in-built material models and solution algorithms. These optimal cycles minimize residual stresses, uniformly cure the laminate in the minimum total cure time and satisfy the constraint of the minimum value, 0.96, of the DoC. With the effective transverse modulus of the lamina being a monotonically increasing function of the DoC, it has the maximum value consistent with the prescribed DoC. For a moderately thick laminate of aspect ratio (span/thickness) 12.5, in comparison to the MRCC, one of the optimal cycles reduces residual stresses by 47% and the total cure cycle time from 5 to 4 h. For a thin laminate of aspect ratio 125, one optimal cure cycle reduces the cure-induced curvature by 13% but increases the total time to 7.4 h from 5 h needed for the MRCC. Another optimal cycle reduces the total cure cycle time to 2 h without affecting the DoC by curing the laminate at higher temperatures but increases the induced curvature by 8% from that produced by the MRCC. Thus, one can find optimal cure cycles to meet the desired objectives.

Declaration of Conflicting Interests

The author(s) declared no potential conflicts of interest with respect to the research, authorship, and/or publication of this article.

Funding

The author(s) disclosed receipt of the following financial support for the research, authorship, and/or publication of this article: RCB's work was partially supported by the Army Contract No. W91CRB-13-C-0048 with Virginia Polytechnic Institute and State University. PHS and RCB gratefully acknowledge Convergent Technologies' allowing us to freely use the software, COMPRO, for almost one year after the paid period expired. The views expressed in this paper are those of authors and do not reflect opinions of either the funding organization or Virginia Tech.

References

1. Purslow D and Childs R. Autoclave moulding of carbon fibre-reinforced epoxies. *Composites* 1986; 17: 127–136.
2. Holl MW and Rehfield LW. An evaluation of the current status of automated process control for thermosetting composites. Composite materials: testing and design, ASTM STP 1120, 1992, 308–319. West Conshohocken, PA: ASTM, 1992, pp.308–319.
3. Hubert P and Poursartip A. A review of flow and compaction modelling relevant to thermoset matrix laminate processing. *J Reinf Plast Compos* 1988; 17: 286–318.
4. Costa VAF and Sousa AC M. Modeling of flow and thermo-kinetics during the cure of thick laminated composites. *Int J Therm Sci* 2003; 42: 15–22.
5. Loos AC and Springer GS. Curing of epoxy matrix composites. *J Compos Mater* 1983; 17: 135–169.
6. Bogetti TA and Gillespie JW. Two-dimensional cure simulation of thick thermosetting composites. *J Compos Mater* 1991; 25: 239–273.
7. Bogetti TA and Gillespie JW. Process-induced stress and deformation in thick-section thermoset composite laminates. *J Compos Mater* 1992; 26: 626–660.
8. Guo Z-S, Du SY and Zhang BM. Temperature field of thick thermoset composite laminates during cure process. *Compos Sci Technol* 2005; 65: 517–523.
9. Ciriscioli PR and Wang Q. Springer GS. Autoclave curing – comparisons of model and test results. *J Compos Mater* 1992; 26: 90–102.
10. Hojjati M and Hoa SV. Curing simulation of thick thermosetting composites. *Compos Manuf* 1994; 5: 159–169.
11. Esposito L, Sorrentino L, Penta F, et al. Effect of curing overheating on interlaminar shear strength and its modelling in thick FRP laminates. *Int J Adv Manuf Technol* 2016; 87: 2213–2220.
12. Sorrentino L, Esposito L and Bellini C. A new methodology to evaluate the influence of curing overheating on the mechanical properties of thick FRP laminates. *Compos B Eng* 2017; 109: 187–196.
13. White SR and Kim YK. Staged curing of composite materials. *Compos A Appl Sci Manuf* 1996; 27: 219–227.
14. Kim JS and Lee DG. Development of an autoclave cure cycle with cooling and reheating steps for thick thermoset composite laminates. *J Compos Mater* 1997; 31: 2264–2282.
15. Oh JH and Lee DG. Cure cycle for thick glass/epoxy composite laminates. *J Compos Mater* 2002; 36: 19–45.
16. White SR and Hahn HT. Process modeling of composites materials: residual stress development during cure. Part I. Model formulation. *J Compos Mater* 1992; 26: 2402–2422.
17. White SR and Hahn HT. Process modeling of composites materials: residual stress development during cure. Part II. Experimental validation. *J Compos Mater* 1992; 26: 2423–2453.
18. White SR and Hahn HT. Cure cycle optimization for the reduction of processing-induced residual stresses in composite materials. *J Compos Mater* 1993; 27: 1352–1378.
19. Gopal AK, Adali S and Verijenko VE. Optimal temperature profiles for minimum residual stress in the cure process of polymer composites. *Compos Struct* 2000; 48: 99–106.
20. Li M, Zhu Q, Geubelle PH, et al. Optimal curing for thermoset matrix composites: thermochemical considerations. *Polym Compos* 2001; 22: 118–131.
21. Pantelelis N, Vrouvakis T and Spentzas K. Cure cycle design for composite materials using computer simulation and optimisation tools. *Forschung im Ingenieurwesen* 2003; 67: 254–262.
22. Jahromi PE, Shojaei A and Pishvaie SMR. Prediction and optimization of cure cycle of thick fiber-reinforced composite parts using dynamic artificial neural networks. *J Reinf Plast Compos* 2012; 31: 1201–1215.
23. Vafayan M, Ghoreishy MHR, Abedini H, et al. Development of an optimized thermal cure cycle for a complex-shape composite part using a coupled finite element/genetic algorithm technique. *Iranian Polym J* 2015; 24: 459–469.
24. Pillai VK, Beris AN and Dhurjati PS. Implementation of model-based optimal temperature profiles for autoclave curing of composites using a knowledge-based system. *Ind Eng Chem Res* 1994; 33: 2443–2452.
25. Rai N and Pitchumani R. Optimal cure cycles for the fabrication of thermosetting matrix composites. *Polym Compos* 1997; 18: 566–581.
26. Johnston AA. An integrated model of the development of process-induced deformation in autoclave processing of composite structures. Doctoral Dissertation, University of British Columbia, 1997.
27. Hubert P. Aspects of flow and compaction of laminated composite shapes during cure. PhD Thesis, The University of British Columbia, Vancouver, Canada, 1996.
28. Carlone P and Palazzo GS. Thermo-chemical and rheological finite element analysis of the cure process of thick carbon-epoxy composite laminates. *Int J Mater Form* 2009; 2: 137–140.
29. Kim KS and Hahn HT. Residual stress development during processing of graphite/epoxy composites. *Compos Sci Technol* 1989; 36: 121–132.

30. Sun CT and Li S. Three-dimensional effective elastic constants for thick laminates. *J Compos Mater* 1988; 22: 629–639.
31. Bogetti TA, Hoppel CP and Drysdale WH. Three-dimensional effective property and strength prediction of thick laminated composite media. MD: Army Research Lab Aberdeen Proving Ground, 1995.
32. Madhukar MS. Cure cycle optimization in polymer composites (No. 121-01-13-070-000-02). Knoxville: Tennessee University, Department of Mechanical and Aerospace Engineering, 2000.
33. Morris MD. Factorial sampling plans for preliminary computational experiments. *Technometrics* 1991; 33: 161–174.
34. Saltelli A, Chan K and Scott EM. *Sensitivity analysis. Wiley series in probability and statistics*. New York: Wiley, 2000.
35. Konak A, Coit DW and Smith AE. Multi-objective optimization using genetic algorithms: a tutorial. *Reliabil Eng Syst Saf* 2006; 91: 992–1007.
36. Mitchell M. *An introduction to genetic algorithms*. Cambridge: MIT Press, 1998.
37. Antoine GO and Batra RC. Optimization of transparent laminates for specific energy dissipation under low velocity impact using genetic algorithm. *Compos Struct* 2015; 124: 29–34.
38. Conn AR, Gould NIM and Toint PhL. A globally convergent augmented Lagrangian algorithm for optimization with general constraints and simple bounds. *SIAM J Numer Anal* 1991; 28: 545–572.
39. Conn AR, Gould NIM and Toint PhL. A globally convergent augmented Lagrangian barrier algorithm for optimization with general inequality constraints and simple bounds. *Math Comput* 1997; 66: 261–288.
40. Noraini MR and Geraghty J. Genetic algorithm performance with different selection strategies in solving TSP. In: *Proceedings of the World Congress on Engineering*. Vol. II. London, UK: WCE, 2011.
41. White SR and Kim YK. Process-induced residual stress analysis of AS4/3501-6 composite material. *Mech Compos Mater Struct Int J* 1998; 5: 153–186.

Appendix

Properties of graphite/epoxy composite

For the epoxy matrix, the heat of reaction, $H_r = 4.74 \times 10^5$ J/kg, and the cure rate is given by[4,28]

$$\frac{dc}{dt} = \begin{cases} (B_1 + B_2 c)(1-c)(0.47-c), & c \leq 0.3 \\ B_3(1-c), & 1 \geq c > 0.3 \end{cases} \tag{7}$$

where

$$B_i = A_i e^{-\frac{\Delta E_i}{RT}} \tag{8}$$

Table 6. Parameters for the epoxy resin kinetics model.

Parameter (units)	Value
A_1 (min^{-1})	2.10×10^9
A_2 (min^{-1})	-2.01×10^9
A_3 (min^{-1})	1.96×10^5
ΔE_1 (J/mol)	8.07×10^4
ΔE_2 (J/mol)	7.78×10^4
ΔE_3 (J/mol)	5.66×10^4

Table 7. Material parameters for fibers and resin.[28]

Property	graphite fiber	epoxy resin
Mass density, ρ (kg/m^3)	1790	1260
Specific heat, C_p (J/kg-K)	712	1260
Thermal conductivity, K (W/m-K)	$K_1 = 26$, $K_2 = 2.6$	0.167

Here A_i is a constant, ΔE_i the activation energy, T the temperature in K, and R = 8.31 J/mol-K the universal gas constant. Values assigned to various parameters in equation (7) are given in Table 6.

In Table 7, we have listed values of material parameters for the graphite/epoxy composite constituents used for the thermo-chemical analysis. The fibers are assumed to be transversely isotropic about the longitudinal axis and the matrix to be isotropic. Resin properties listed in Table 7 are assumed not to vary with the temperature and the DoC.

The resin viscosity is assumed to vary with the temperature and the DoC as follows[4,28]:

$$\mu = \mu_\infty \exp\left(\frac{U}{RT} + Zc\right) \tag{9}$$

where $\mu_\infty = 7.93 \times 10^{-14}$ Pa·s, $U = 9.08 \times 10^4$ J/mol, and $Z = 14.1$ for the 3501-6 resin.

The permeabilities of the resin impregnated fiber-bed are given by the following Kozeny–Carman equation.[4,28]

$$S_{xx} = \frac{r_f^2}{4Q_{xx}} \frac{\left(1-V_f\right)^3}{V_f^2} \text{ and }$$
$$S_{yy} = S_{zz} = \frac{r_f^2}{4Q_{zz}} \frac{\left[\left(V_a/V_f\right)^{1/2} - 1\right]^3}{V_a/V_f + 1} \tag{10}$$

Table 8. Mechanical properties of fibers and resin.

Property	Graphite fiber[41]	Epoxy resin[7]
Young's modulus (GPa)	$E_1 = 207$, $E_2 = E_3 = 20.7$	$E_r = (1-c)E_r^0 + cE_r^\infty$, $E_r^0 = 3.447\,x\,10^{-3}$, $E_r^\infty = 3.447$
Poisson's ratio	$\nu_{12} = \nu_{13} = 0.2$, $\nu_{23} = 0.3$	$\nu_r = 0.35$
Shear modulus (GPa)	$G_{12} = G_{13} = 27.6$	$G_r = E_r/2(1+\nu_r)$
Coefficient of thermal expansion ($^\circ C^{-1}$)	$\alpha_{11} = -9 \times 10^{-7}$, $\alpha_{22} = \alpha_{33} = 7.2 \times 10^{-6}$	$\alpha = 5.76 \times 10^{-5}$
Total specific volume shrinkage	–	$v_{sh}^T = 0.03$
The resin volumetric strain	–	$e_v = c\,v_{sh}^T$

Table 9. Coefficients of the least squares fit for the non-dimensional curvature, $\bar{\chi}$, and the , c.

	n = 120		*n* = 180	
Coefficient	$\bar{\chi}$	c	$\bar{\chi}$	c
a_0	36.1857	0.7422	34.4374	0.6641
a_1	−1.4685	0.0499	−0.1366	0.1195
a_2	22.2057	0.3359	26.4160	0.4755
a_3	1.5653	0.0477	−3.3648	−0.0848
a_4	−4.1035	−0.0132	−5.4003	−0.0096
a_5	−3.7583	0.0164	−2.5902	0.0843
a_6	13.1165	0.4136	17.3864	0.5386
a_7	−0.8323	−0.0031	2.7155	0.0852
a_{11}	5.1984	0.0379	4.2362	−0.0073
a_{12}	−6.1622	−0.0479	−9.1867	−0.1145
a_{13}	−2.7347	−0.0094	−0.2589	0.0718
a_{14}	−0.3826	−0.0055	2.0864	0.0604
a_{15}	3.3886	−0.0226	2.7587	−0.0461
a_{16}	−1.6462	−0.0421	−3.7861	−0.1204
a_{17}	−0.9024	−0.0073	−0.5307	−0.0247
a_{22}	−6.2945	−0.1300	−7.5665	−0.1887
a_{23}	−0.7302	−0.0212	0.8659	0.0314
a_{24}	−1.3322	0.0138	−1.0696	0.0130
a_{25}	−4.4137	−0.0250	−5.1635	−0.0533
a_{26}	−7.1244	−0.2159	−10.5731	−0.3145
a_{27}	0.3968	0.0182	0.5045	0.0129
a_{33}	−0.3648	−0.0117	−0.4239	−0.0326
a_{34}	0.9244	0.0301	0.0854	0.0047
a_{35}	−1.5445	−0.0482	1.9439	0.0486
a_{36}	−1.2930	−0.0347	1.8803	0.0589
a_{37}	0.7984	0.0234	0.2603	0.0052
a_{44}	0.3504	−0.0275	1.1750	−0.0167
a_{45}	3.2530	0.0619	1.6104	−0.0061
a_{46}	−0.2140	−0.0013	0.1834	−0.0058
a_{47}	0.0814	0.0062	0.3155	0.0052
a_{55}	2.1816	0.0364	1.6255	0.0061
a_{56}	−1.6800	−0.0431	−2.5070	−0.0704
a_{57}	0.3495	0.0136	−1.2736	−0.0297
a_{66}	−5.1284	−0.1773	−7.1425	−0.2235
a_{67}	0.6996	0.0121	−0.8241	−0.0179
a_{77}	0.3535	−0.0255	−1.4301	−0.0458

in which the fiber radius $r_f = 4\,\mu m$, the modified Kozeny constants, determined experimentally, are $(Q_{xx}, Q_{zz}) = (0.7, 0.2)$, and the value of V_a determined experimentally is 0.8.

The fiber-bed elastic constants in the material principal axes (y_1, y_2, y_3) with the y_1-axis being the axis of transverse isotropy are given by[27]

$E_1^{fb} = 117\,\text{GPa}$, $E_2^{fb} = E_3^{fb} = 7.92\,\text{MPa}$, $G_{12}^{fb} = G_{13}^{fb} = G_{23}^{fb} = 2.64\,\text{MPa}$, $\nu_{12}^{fb} = \nu_{13}^{fb} = 0$.

As pointed out by Hubert,[27] during the consolidation of the laminate, the coupling between the longitudinal and the transverse strains is found to be negligible and hence, Poisson's ratios $\nu_{12}^{fb} = \nu_{13}^{fb}$ are assumed to be zero.

The mechanical properties of the graphite fibers and the epoxy resin are listed in Table 8.

As pointed out by White and Kim[41] neglecting the cure dependency of Poisson's ratio of the epoxy resin has very little effect on the development of either Young's or the shear modulus during cure and thus the accuracy of the computed residual stresses. Hence, Poisson's ratio has been assumed to be constant.

Table 10. Coefficients of the least squares fit for σ_{xx}^{max} and c_{min}.

Coefficient	σ_{xx}^{max} (MPa)	c_{min}
a_0	107·3396	0·7616
a_1	−8.8549	0·0641
a_2	85·3424	0·4048
a_3	−11.1745	−0.0500
a_4	−30.1225	−0.0437
a_5	−28.3194	0·0405
a_6	45·8053	0·3828
a_7	131·2704	0·0630
a_{11}	14·6480	−0.0001
a_{12}	−37.7132	−0.0950
a_{13}	−9.7805	0·0545
a_{14}	6·6804	0·0647
a_{15}	23·2118	−0.0328
a_{16}	−8.5059	−0.0835
a_{17}	2·8845	−0.0021
a_{22}	−26.3671	−0.1685
a_{23}	−3.2888	0·0204
a_{24}	−9.6963	0·0131
a_{25}	−22.0528	−0.0452
a_{26}	−36.7483	−0.2561
a_{27}	26·3145	0·0069
a_{33}	4·5424	−0.0234
a_{34}	−1.5752	−0.0005
a_{35}	10·4587	0·0330
a_{36}	3·9244	0·0385
a_{37}	4·5996	−0.0054
a_{44}	6·6545	−0.0006
a_{45}	8·7501	0·0029
a_{46}	2·8917	0·0154
a_{47}	11·5804	0·0012
a_{55}	9·8958	0·0163
a_{56}	−9.1496	−0.0407
a_{57}	−2.0563	−0.0178
a_{66}	−14.6906	−0.1614
a_{67}	−0.9078	−0.0034
a_{77}	−102.7189	−0.0427

Coefficients of model fits for the output parameters of the optimization study

The values of 36 coefficients in equation (5) for model fits for the non-dimensional curvature and the DoC obtained with $n = 120$ and 180 are given in Table 9.

The values of 36 coefficients in equation (5) for model fits for σ_{xx}^{max} and c_{min} are listed in Table 10.